Investigation of Tribological Behavior and Lubrication Mechanisms of Zinc Oxide under Poly α-olefin Lubrication Enhanced by the Electric Field

Yaowen Chen, Min Ji, Feichi Zhang, Jing Li, Haijun Pan, Yujie Zhao, Zhen Zhang, and Lin Liu*

ABSTRACT: The electric field induces complex effects on the tribological properties of zinc oxide (ZnO) under lubricated conditions, particularly at the nanoscale, where the friction process and mechanism remain unclear. In this paper, the tribological behaviors of ZnO under the lubrication of poly α-olefins (PAO) were investigated by molecular dynamics (MD) simulations with reactive force field (ReaxFF). The results reveal a significant enhancement in the tribological performances of ZnO with the application of the electric field, resulting in a 58.6% reduction in the coefficient of friction (COF) from 0.193 at 0 V/Å to 0.080 at 0.1 V/Å. This improvement can be attributed to the weakening of interfacial interaction, evidenced by a reduction in the number of C−O covalent bonds under the influence of the electric field, along with the formation of an adsorption film due to applied load and shear effects. Notably, the effect of the electric field and applied load extends the impact of interface slip on the tribological performance of ZnO. Overall, this study provides a comprehensive understanding of the impact of the electric field on reducing the friction of ZnO-based structured models, shedding light on explaining their tribological properties and lubrication mechanisms.

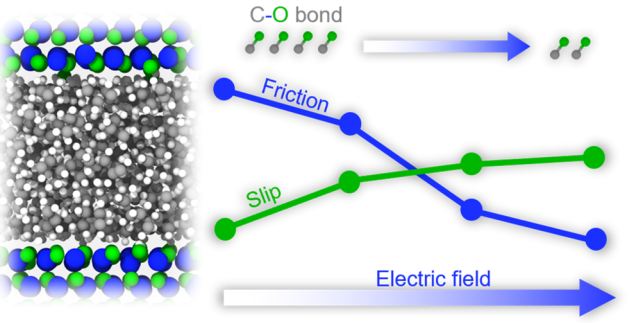

INTRODUCTION

Piezoelectric semiconductor materials (e.g., ZnO, GaN, ZnTe, etc.) have attracted much attention[1−3] due to their unique properties,[4−6] such as dual piezoelectric and semiconductor properties. Among these materials, ZnO has been widely used in triboelectric nanogenerators[4] and surface coatings since they exhibit excellent flexibility, biocompatibility, and good lubricity.

The tribological behaviors of ZnO have been widely investigated and are associated with its intrinsic single-crystal structure. It was found that the nanocrystalline grain structure and oxygen stoichiometry contribute to the low COF of ZnO films.[7−9] After the high-temperature annealing process, the reconstruction occurred on the (0001) surface, forming defects and adsorbates, contributing to the low friction of the ZnO single crystal.[10] Goto revealed that the piezoelectric effect helps to improve the tribological performance of the ZnO films in a vacuum or at high temperatures.[11,12] Sasaki et al.[4] recognized that the friction force of B-doped ZnO strongly depends on the piezoelectric force of nanodomains. In our previous study, based on classical MD simulations, it has been demonstrated that the interaction between ZnO and lubricants can enhance the tribological performance of the system.[13,14] They focused on studying by traditional experimental and simulating methods, whereas the tribological performance of ZnO at the atomic scale is still unclear, especially the deeper understanding of the tribology interface.

Interest in applying the external electric field on a lubrication system to adjust its frictional properties has found to be prevalent in recent years. For instance, Peng et al.[15] showed that the mechanism of $MoSe_2$ under the external electric field is related to electrostatic force and adsorption. More recently, Chen et al.[16] indicated that the electrostatic interaction plays a dominant role in the improvement of nanotribological performance under the external electric field. Gao et al.[17] investigated the coupling effects of shear and electric field on friction, and the results indicated that the friction force decreases with the voltage increasing in the low-speed range and the external electric field rarely works in the high-speed range. These friction experiments show the effect of the external electric field on the tribological performance. However, the influence of the external electric field on ZnO nanotribological performance using the MD simulation has

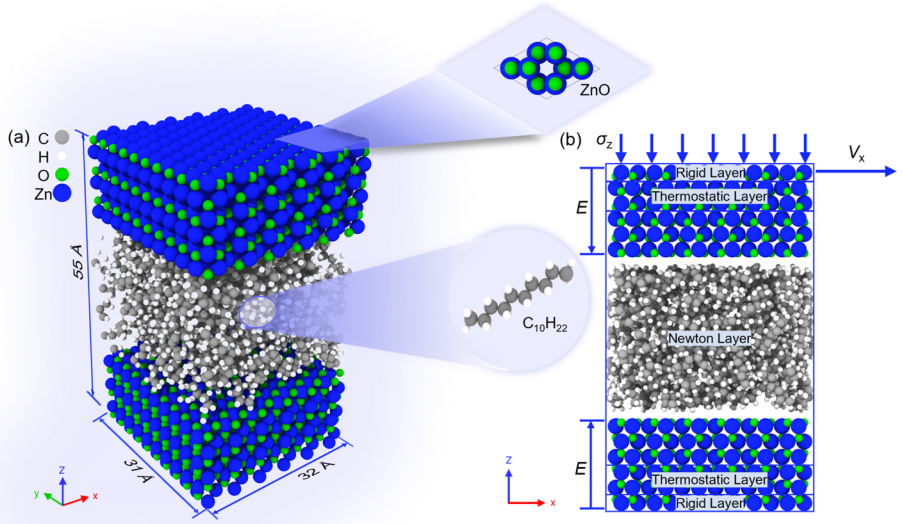

Figure 1. (a) Configuration of the ZnO−PAO−ZnO model in the MD simulation, and the size of the model is 32 × 31 × 55 Å^3. (b) 2D friction model showing three parts of the system: rigid layer, thermostatic layer, and newton layer. The direction of the external electric field is along the *z*-axis.

rarely been reported. Moreover, the effect of the electric field on chemical bonding at the interface of ZnO is not well understood at the atomic scale.

ReaxFF MD simulations can describe the breaking and formation of interatomic bonds and thus can be used to explain the occurrence of tribochemical reactions in materials.[18−20] According to ReaxFF MD simulations, Yu et al.[21] revealed the significance of shear stress in a tribo-oxidation reaction. Wang et al.[22] found that the formation of interfacial C−Fe bonds has a remarkable influence on the tribological performances of steel sliding contacts. Hence, it is considered that this simulation approach is a superior choice for investigating the nanotribological performances of ZnO at the atomic level.

This study aims to investigate the tribological behavior of ZnO under the external electric field using ReaxFF MD simulations. By varying the magnitude of the applied electric field and load at high temperatures, the nanofriction mechanism of ZnO will be elucidated, with a focus on analyzing the COF, structural characteristics, and tribochemical reactions at the interface. This research will contribute to a comprehensive understanding of the tribological performance of ZnO, further enhancing our mechanistic insights.

SIMULATION MODEL AND METHODS

In this study, both ZnO and lubricant (i.e., PAO) models were constructed by Large-scale Atomic/Molecular Massively Parallel Simulator (LAMMPS)[23] and Packmol.[24] The ZnO model was the arrangement of a ZnO single crystal, with the $(000\bar{1})$ plane as the friction interface.[13] To simplify the model of PAO, the lubricant was composed of 20 linear polydecene molecular chains with five polymerization degrees.[25,26] The size of the model was 32 × 31 × 55 Å^3.

Figure 1 presents the configuration and schematic diagram of the friction model. As shown in Figure 1a, the simulation model was periodic along with the *x* and *y* axes and nonperiodic along the *z* direction. It can be seen that the ZnO layer was divided into three parts, including the rigid layer, the thermostatic layer, and the Newton layer. The bottom rigid layer was fixed throughout the whole simulation process, the thermostatic layer was set to keep the system temperature constant, and the lubricant layer was set as the newton layer, where the molecule was able to move under the load. The normal load (*z*-direction) and velocity (*x*-direction) were applied to the top layer.

The whole simulation process was divided into three stages, relaxation stage, loading stage, and sliding stage: (i) In the relaxation stage, the thermostatic layer imposed the Nose−Hoover thermostat to conduct heat generated because of loading shock. Atoms in the Newton layer using the NVE ensemble were able to move freely and subjected to a constant loading pressure on the system in this stage.[27,28] The simulation process lasted 2 ns. (ii) The top rigid layer applied a normal load to compress the system until the energy was stable and then kept this process lasting 0.5 ns. The bottom rigid layer was fixed during the whole stage. (iii) The upper and bottom ZnO layers were applied with the constant electric field (shown in Figure 1b) until the system was stable, and then a sliding velocity V_x was applied to the upper rigid layer along the *x* direction. Note that the normal load was kept constant at the upper rigid layer when the velocity was applied.

All simulations were performed in open source software LAMMPS,[23] and then the model was visualized in the Open Visualization Tool (OVITO).[29] In this work, combining previous C/H/O and Zn/O/H potentials, proposed by Sengul,[30] the reactive force field was selected, which was used to describe the interaction of the solid/liquid interface. The core of the ReaxFF reaction force field is the expression of the bond order, as follows:[31]

$$\begin{aligned} BO'_{ij} &= BO^{\sigma}_{ij} + BO^{\pi}_{ij} + BO^{\pi\pi}_{ij} \\ &= \exp\left[P_{bo1}\left(\frac{r_{ij}}{r_o^{\sigma}}\right)^{p_{bo2}}\right] + \exp\left[P_{bo2}\left(\frac{r_{ij}}{r_o^{\pi}}\right)^{p_{bo4}}\right] \\ &\quad + \exp\left[P_{bo5}\left(\frac{r_{ij}}{r_o^{\pi\pi}}\right)^{p_{bo6}}\right] \end{aligned} \tag{1}$$

where BO^{σ}_{ij}, BO^{π}_{ij}, and $BO^{\pi\pi}_{ij}$ are the bond-order contributions from σ bonds, π bonds, and double π bonds, respectively. The p_{bo} variables are the parameters used in the force field to describe bonding interactions. r_{ij} is the atomic distance between the *i*th and *j*th atoms, and various r_o values are the optimal bond radii. To describe electrostatic interaction, the charge equilibration process was ensured by the qeq/reax method at each time step,[32] the convergence of

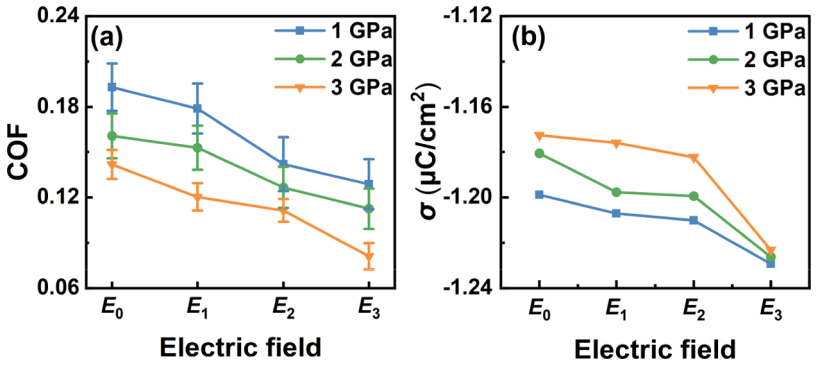

Figure 2. Evolution of (a) COF and (b) surface charge density with different electric field intensities. σ represents the surface charge density of upper slab ZnO that contacted with PAO, which was achieved at the end of the simulation.

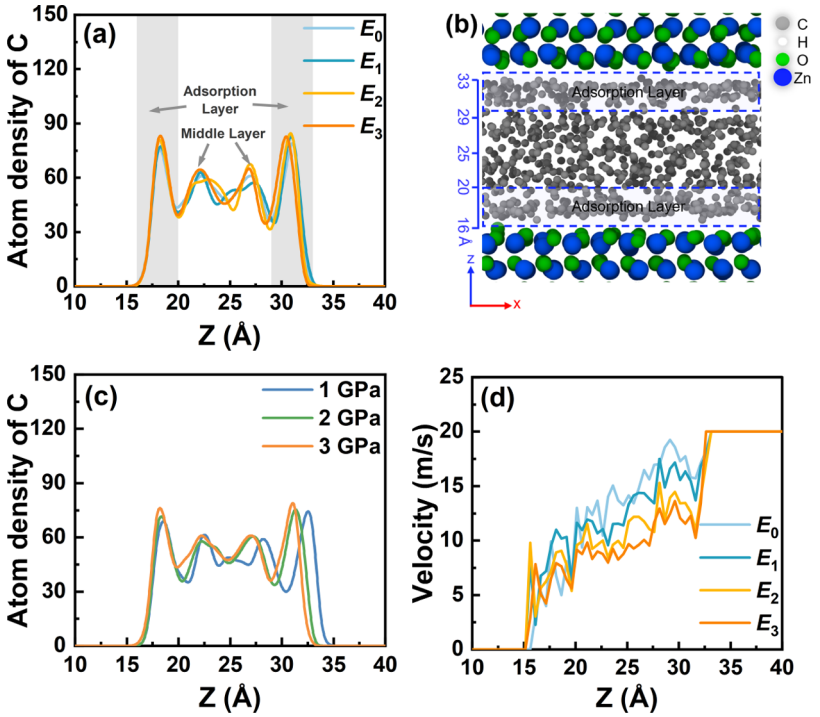

Figure 3. Distribution of C element along the cross section of the model under (a) different electric field intensities and (c) normal loads and (b) the snapshot of C element distribution in the built model at 3 GPa. The dashed blue rectangle in (b) showing the adsorption layer corresponding to the gray area in (a). For easy observation, the H atoms were hidden in the lubricant layer. (d) The velocity distribution of the system along the normal load direction. All results were obtained from the end of the simulation.

accuracy was 1×10^{-6} kcal/mol, and the time step was 0.25 fs. The velocity verlet algorithm was used to solve the motion of particles.[33] Based on the fact that the carbon tribofilm was formed under an extreme loading condition,[34] the applied load σ_z on the top rigid layer was set to three values, 1, 2, and 3 GPa, respectively.[35,36] The sliding velocity V_x was set to 20 m/s with a simulation time of 250 ps. In this study, four intensity values E (i.e., $E_0 = 0$ V/Å, $E_1 = 1 \times 10^{-3}$ V/Å, $E_2 = 1 \times 10^{-2}$ V/Å, and $E_3 = 1 \times 10^{-1}$ V/Å) were applied to ZnO. The temperature of the thermostatic layer was set at 500 K based on the previous study that ZnO can achieve excellent tribological performance at a high temperature on the vacuum.[12] The temperature is smaller than the onset temperature of base oil decomposition to simulate the conditions at a high temperature and fasten the reactions of the system.[37] In addition, a high temperature helped with accelerating the speed of the chemical reaction without changing the reaction pathway and the deformation of species.

During the friction process, the friction force was collected by calculating the atom force of the upper rigid layer and the bottom rigid layer along the x direction, and then the COF was calculated by the following expression:[38]

$$\mu = \frac{\langle F_{xz} \rangle}{\langle F_z \rangle} \tag{2}$$

where F_{xz} and F_z represent the atom lateral force and the normal force, respectively. Besides, the distribution of C atoms under different conditions is calculated. The interface slip ratio was calculated by the following formula to analyze its relationship with the applied load and electric field:[39,40]

$$S = \frac{V_s - V_l}{V_s} \tag{3}$$

where V_s and V_l represent the velocity of ZnO and lubricant near the interface at the end of the simulation, respectively. For achieving relatively accurate results, F_{xz} and F_z were obtained from the last 10 ps of simulation. Additionally, the mean squared displacement (MSD)

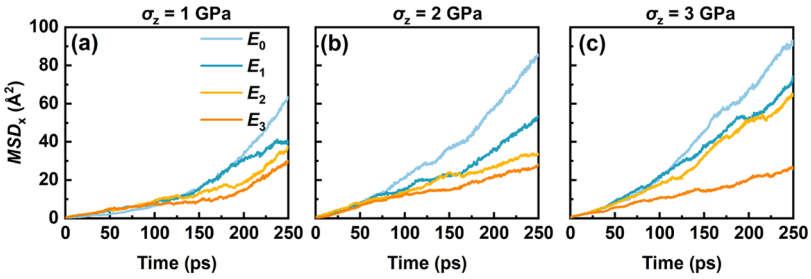

Figure 4. Evolution of MSD of lubricants over time in different cases: (a) σ_z = 1 GPa, (b) σ_z = 2 GPa, and (c) σ_z = 3 GPa.

along the x direction of lubricant during the sliding stage was computed by the following equation:[41]

$$\mathrm{MSD}(t) = \langle |r_t(t) - r_t(0)|^2 \rangle \quad (4)$$

where $r_i(t)$ and $r_i(0)$ represent the displaced position of molecules and the original position before the sliding stage, respectively. The distribution of the C atom was obtained at the end of the simulation. In order to explore the change at the solid/liquid interface and the structure of the lubricant, we counted the number of C−O covalent bonds.

RESULTS AND DISCUSSION

Tribological Performance. Figure 2a shows the evolution of the ZnO friction coefficient (by eq 2) with the change of electric field intensity at 500 K. It can be seen that the COF of ZnO fluctuates slightly, with a generally decreasing trend under increasing electric field intensity. The COF was approximately 0.193 without an external electric field at the load of 1 GPa and decreased to 0.129 with an electric field intensity of 0.1 V/Å. At 2 GPa, the COF decreased from 0.161 without an external electric field to 0.113 at 0.1 V/Å. Similarly, the COF was around 0.168 without electric field at the load of 3 GPa and reduced to 0.081 with an electric field intensity of 0.1 V/Å. The presented findings reveal that the tribological characteristics of ZnO undergo alterations when subjected to an electric field. It is important to note that the COF is influenced by the chosen number of output frequencies, repetitions, and averaging steps in the model, with error bars plotted in the curves to illustrate deviations.[42] Figure 2b shows the surface charge density of ZnO under different electric field intensities. The ZnO crystal lattice was distorted as a result of the applied load, causing electrical polarization and decreasing the surface charge density. Under the influence of the electric field, the surface charge density gradually decreased. It was obvious when the electric field intensity increased to 0.1 V/Å. This result suggests that the Coulomb repulsion between ZnO and PAO increases under the effect of an electric field, which contributes to the decrease in shear resistance. Additionally, the COF of ZnO decreases with increasing load without applying the electric field, which is in agreement with the results of the previous studies.[11,12] Previous experimental studies proposed that, based on the piezoelectric property of crystal nanodomains, the normal load can alter the polar part of the surface energy, thereby decreasing the COF of ZnO. It is inferred that the electric field enhances the effect of the normal load, leading to a reduction in COF. Consequently, the electric field effectively contributes to the enhancement of tribological performances. Interestingly, when the electric field intensity was 0.1 V/Å, the difference in surface charge density was small but the difference of COF was large.

Structural Characteristics. The structure of boundary films formed by lubricant molecules plays a crucial role in determining friction and wear reduction performance.[43,44] To better understand the structural features of the carbon-based tribofilm under heavy load conditions, the number density distribution of C atoms has been counted. Figure 3a illustrates that under a pressure of 3 GPa, two atomic layers were formed for carbon, with the adsorption layer positioned close to ZnO, while the middle layer was farther away. The formation of adsorption layers is attributed to atomic attractions from ZnO. Because of the existence of PAO, direct contact between ZnO friction pairs was avoided. As shown in Figure 3c, with increasing normal load, PAO molecules undergo compression and C atoms present a dense state, exhibiting a solid-like phenomenon, which is characterized by the formation of a layered structure. Furthermore, it also indicates that the adsorption film formed by PAO provides an excellent bearing performance. Tighter adsorption between internal lubricant molecules occurred due to the shearing effect. In conjunction with Figure 3b, it is evident that the number of C atoms near the boundary is higher, indicating a greater concentration compared to the layer with a lower concentration. This result indicates that lubricants tend to move toward the boundary of the ZnO layer in the sliding process and form an adsorption layer. However, it is found that the electric field has a weak influence on the distribution of atom density in Figure 3a, which is probably related to the interaction between the interface and lubricant. Consequently, the formation of an adsorption film under the applied load emerges as a key factor contributing to friction reduction. Figure 3d shows the distribution of the PAO velocity along the normal load direction. It can be observed that there is a velocity difference between ZnO and PAO, and this difference is gradually obvious with the increase in the electric field intensity. Therefore, the electric field has a weakening effect on the movement ability of PAO. It is necessary to analyze the motion of PAO.

In order to explore the change of the lubricant motion under the influence of the electric field, the MSD of the lubricant has been counted by eq 4. It is reported that the MSD reflects the diffusive motion of particles, which affects the frictional performance.[45] Figure 4 depicts the change in the MSD of PAO molecules along the x direction at different loads and electric field intensities. The diffusion trend of PAO molecules can be intuitively observed with a significant change in the MSD slope. The simulation results show that the diffusion ability of PAO gradually increases with the increase in applied load under the condition of constant electric field intensity. For instance, the diffusion of PAO under the 3 GPa load (Figure 4c) is superior to that under the 1 GPa load (Figure 4a) at an electric field intensity of 0 V/Å. The long chain length of PAO

molecules makes it easier for them to form a lubricating film adsorbed on the solid surface. And then, PAO molecules gradually diffuse as the shear motion proceeds. It is worth noting that the changes in all MSD curves are relatively slow within the first 100 ps when the load is 1 GPa, indicating a basically consistent diffusion trend of PAO. After 100 ps, the differences between the MSD curves gradually become apparent and the diffusion performance of PAO changes to varying degrees. This change occurs at a time point of about 75 ps when the load grows to 2 GPa, and it happens at a time point of about 50 ps when the load increases to 3 GPa. The self-diffusion rate of PAO is relatively slow under the constraint of heavy loads. Additionally, the interaction between PAO and ZnO is strengthened because of the compressed space, which promotes PAO adsorption on the surface of ZnO. Furthermore, with the introduction and increase in electric field intensity, the molecules' motion tends to weaken, which contributes to the stability of the adsorption film.

Figure 5 shows the diffusivity of PAO under different electric field intensities and normal loads. With the introduction and

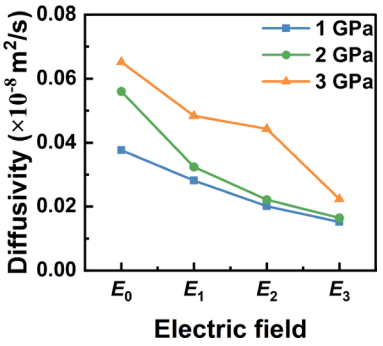

Figure 5. Diffusivity of PAO under different electric field intensities and normal loads.

improvement of the electric field, the diffusivity of PAO decreases, suggesting that the electric field weakens the ability of PAO to move along the shear direction. With the increase of load, the diffusivity of PAO gradually increases, so the increase of load enhances the movement ability of PAO along the shear direction. The above results can be attributed to the synergistic effect of shear, heavy load, and electric field. It can be concluded that the electric field indirectly has a weakening effect on the diffusive motion of the molecules in the lubricant and an increase in the electric field intensity (i.e., 0.1 V/Å) could negatively affect the diffusive effect of PAO.

It is widely known that interfacial slip can affect the tribological performance of the system.[46−48] Figure 6 depicts the slip ratio between ZnO and interfacial lubricants under different electric field intensities and loads (calculated in eq 3). The results show that the slip ratio increases with increasing load under constant electric field intensity as the solid-like degree increases at the interface. Higher loads lead to higher velocity of the lubricants, manifested as a higher interfacial slip rate. It is found that the increase in slip ratio is most significant when the electric field intensity is 0 V/Å and less pronounced when the electric field intensity is 0.1 V/Å. The slip ratio increases with increasing electric field intensity and gradually levels off under the same load. For instance, the ratio increased from 0.1656 to 0.2970 at a load of 1 GPa. The intensity of interfacial interaction plays a pivotal role in determining interfacial slip. It has been reported that a weaker solid/liquid

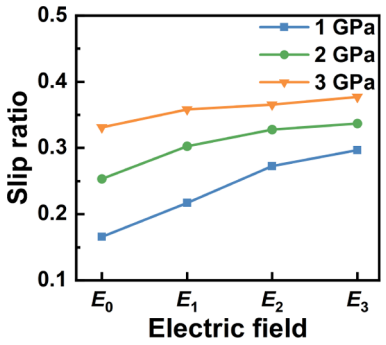

Figure 6. Variation of the slip ratio between ZnO and PAO with different electric field intensities.

interfacial interaction is more conducive to slip.[46,49] It can be inferred that the introduction of the electric field causes a decrease in the solid/liquid interface interaction, consequently leading to an increase in the slip ratio. Combined with the coefficient of friction in Figure 2, it can be found that a higher slip ratio corresponded to a lower coefficient of friction when the electric field intensity gradually increased. Ultimately, the shear resistance of ZnO was decreased under the influence of the slip ratio. Intriguingly, the most substantial increase in slip ratio occurred under a load of 1 GPa, whereas the increase was less pronounced under a load of 3 GPa. This discrepancy can be attributed to the reduction in distance between ZnO and PAO under the heavy load, strengthening the interface interaction. Consequently, the impact of the electric field on interface slip tends to weaken.

Tribochemistry Analysis. For investigating the changes in interfacial interactions, the results of the temporal variation of C−O covalent bonds under an electric field from 0 to 0.1 V/Å and loads of 1 to 3 GPa conditions were determined using statistical analysis of C−O covalent bonds, as shown in Figure 7. The results showed that the number of C−O covalent bonds

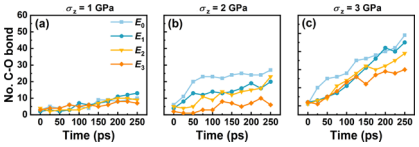

Figure 7. Variation of the number of C−O bonds over time under different applied loads during the sliding process. (a) σ_z = 1 GPa, (b) σ_z = 2 GPa, and (c) σ_z = 3 GPa.

gradually increased during the shear motion process in all conditions. In the beginning, shear motion accelerated the thermal motion of molecules, facilitating the activation energy by PAO molecules and making it easier for the combination of C and O atoms.[50] Subsequently, the distance between O atoms and C atoms became less than the bonding length, creating favorable electronic cloud overlap for electron transfer and inducing the formation of C−O covalent bonds.[51,52] The number of C−O covalent bonds increased with increasing load under the condition of constant electric field intensity. This is due to compression of the space between the wall and lubricant molecules under heavy loads, greatly increasing the probability of bond formation for relevant atoms. It was also found that the number of C−O covalent bonds decreased with increasing electric field intensity when the load was constant, indicating that the electric field hindered the formation of

covalent bonds. Because the existence of an external electric field generated an electric field force, it caused an increase in the distance between some of the O atoms and C atoms and reduced the formation of the C−O covalent bond. Compared with the Figures 2a and 7, it can be found that the lower COF generally corresponds to a lower number of C−O covalent bonds with increasing electric fields. This is due to the decrease in C−O covalent bonds, which weakens the interface interaction and decreases the shear resistance.

Figure 8 shows a snapshot of the friction model with magnified views, showing the generated bonds on the left side

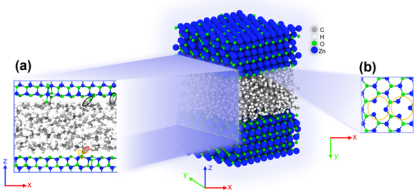

Figure 8. Snapshot of the friction model showing the (a) generation of the C−O and the O−H bonds and (b) breaking of the Zn−O bond at 3 GPa and 0.1 V/Å.

(Figure 8a) and defects on the right side (Figure 8b), respectively. As shown in Figure 8a, three types of covalent bonds were identified on the interface after the sliding process. The first kind of bond was the C−O bond, which was composed of C atoms from PAO molecules and O atoms from the ZnO surface (indicated by black circles in Figure 8a). The second kind of C−O bond is indicated by red circles, where the C atom has not yet entered the bonding distance range. The strong attractive force between C and O causes the O atom to detach from the original surface and combine with the lubricant, forming a covalent bond. The third kind of bond was the C−H bond indicated by yellow circles in Figure 8a, it is observed that H atoms are broken from the carbon chains and then combine with O atoms on the ZnO surface, forming hydroxyl groups.[53] These phenomena confirm the generation and composition of the tribofilm adsorbed on the ZnO surface. Figure 8b shows defects with O atoms detached from the ZnO surface, indicated by yellow circles. Previous studies have reported that defects can affect the tribological performance of the system[54,55] and the mechanism is complex but is not the main focus of this paper. It is worth noting that the ZnO interface structure was unstable at 500 K because the O atoms on the ZnO surface were unsaturated and the coordination number was not sufficient. Figures 9 and 10 present the changing trend toward the number of molecules and species in the lubricant under different loads and electric fields. During the sliding process, the carbon chain on the lubricants was likely to decompose and then form two or multiple smaller molecules, leading to an increase in both the number and type of molecules. It is also observed that electric fields hinder the decomposition of the lubricants, with a relatively slower increase in the number of species with increasing electric fields. For this reason, complete and longer carbon chains were more likely to remain under electric fields, which provide a more stable tribofilm and hence obtain better lubricating abilities, corresponding to the results in Figure 2.

Figure 11 shows a schematic of the lubrication mechanisms of the ZnO−PAO−ZnO model under the external electric field. Based on the discussion above, the formation of the tribofilm on the mated surface contributes to the good lubrication properties of the system. Under the effect of the normal load, the lubricating oil exhibits severe solid-like behavior,[56] enhancing the adsorption stability of the film. Furthermore, the slip ratio between ZnO and PAO near the wall surface increases with the increase of load, which contributes to the decrease in shear resistance of ZnO and then improves the tribological performance of ZnO. However, the powerful interfacial interaction affects the tribological performance of ZnO, which is manifested in the formation of the C−O bond.

The introduction of the electric field hinders the formation rate of the C−O bond. The probability of bonding between C and O atoms at the interface diminishes, resulting in a weakening of the interaction at the interface. Due to the reduced interface interaction, it enhances the interface slip upon introducing the electric field, and the consequent increase in slip ratio contributes to a decrease in the shear resistance of ZnO. Simultaneously, the diffusion degree of PAO along the shear direction decreases. While the electric field indirectly hinders the decomposition of the lubricants and improves the lubrication performance of PAO. This proves to be beneficial in enhancing the overall tribological performance of ZnO. Consequently, apart from the surface adsorption film, the influence of interface slip on the tribological performance of ZnO becomes more pronounced with the introduction of the electric field. In other words, leveraging the coupling of applied load and electric field, the adsorption film and interface slip exhibit a synergistic effect on the tribological performance of ZnO.

In this work, we focused on the influence of the normal load and electric field on the tribological performance of ZnO. However, it is necessary to acknowledge the limitations of this

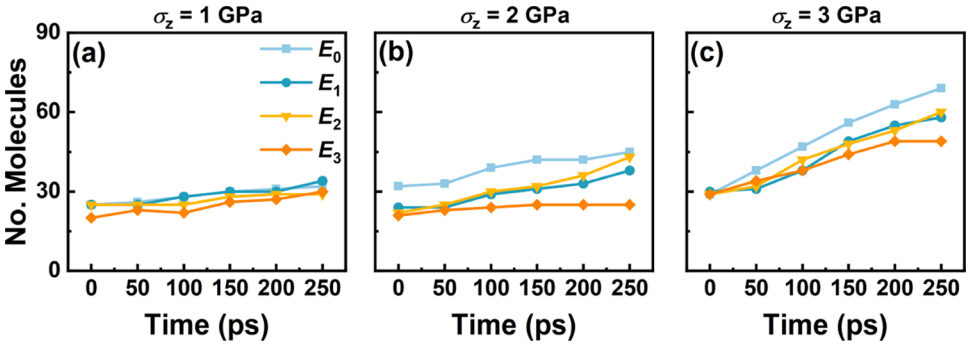

Figure 9. Number of total molecules as a function of time with different applied loads: (a) σ_z = 1 GPa, (b) σ_z = 2 GPa, and (c) σ_z = 3 GPa.

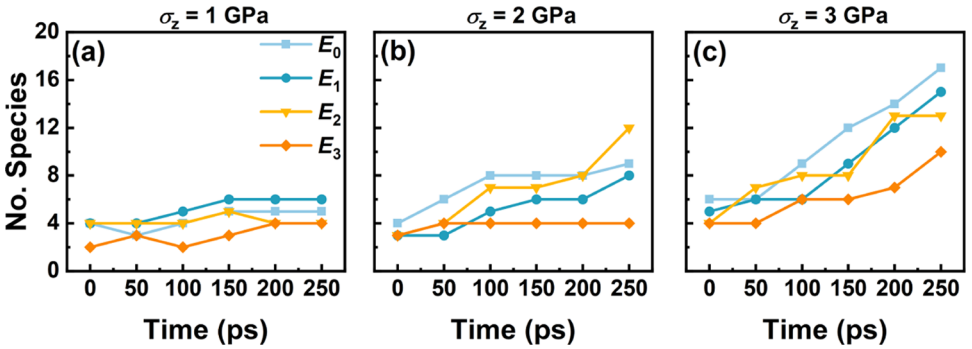

Figure 10. Number of total species as a function of time with different applied loads; (a) σ_z = 1 GPa, (b) σ_z = 2 GPa, and (c) σ_z = 3 GPa.

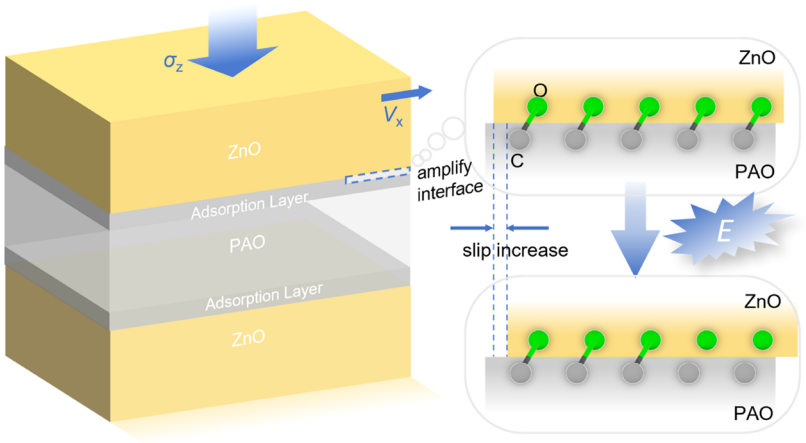

Figure 11. Schematic model for the lubrication mechanisms of the system without and with an electric field.

work. Temperature is an important factor in tribology, but we have not considered the synergistic effect between temperature, normal load, and electric field. It is complex to investigate and needs to be further studied in future work.

CONCLUSIONS

This study explores the influence of the electric field and load on the tribological properties of the ZnO−PAO−ZnO model lubricated with PAO through MD simulations, enhancing our comprehension of its tribological and lubrication mechanisms. The key conclusions can be summarized as follows:

(1) The application of the electric field significantly enhanced the tribological performances of ZnO, as evidenced by a notable 58.6% decrease in the coefficient of friction (COF) from 0.193 at 0 V/Å to 0.080 at 0.1 V/Å. Under the influence of normal load and electric field, the lattice distortion of ZnO occurred, which caused polarization, thus the surface charge density changed, and the Coulomb repulsion between ZnO and PAO was enhanced.

(2) Under the influence of applied load and shear, a lubricating film adhered to the surface of ZnO, delivering exceptional bearing performance and preventing direct contact between the frictional pair. The interface slip between ZnO and PAO occurred and increased with the rise of normal load. At the same time, increased load facilitated the motion of PAO along the shear direction. However, the tribochemical reaction between ZnO and PAO promotes the formation of C−O covalent bonds, which enhances the interfacial interaction and weakens the tribological performance of ZnO.

(3) The introduction of an electric field led to a reduction in the number of C−O covalent bonds, resulting in a weaker interface interaction and an increased slip ratio at the interface. The influence of the electric field on interface slip diminished with an increase in applied load. The electric field impeded the decomposition of lubricants, thereby enhancing the lubrication performance of PAO. In addition, the synergistic effect of the electric field and applied load extended the impact of interface slip on the tribological performance of ZnO. This, in turn, lowered the shear resistance of ZnO, thereby improving its overall tribological performance.

AUTHOR INFORMATION

Corresponding Author

Lin Liu − *School of Mechanical Engineering and Rail Transit, Changzhou University, Changzhou 213164, China;* orcid.org/0000-0002-7728-0317; Phone: +86 519 86334782; Email: liulin@cczu.edu.cn

Authors

Yaowen Chen − *School of Mechanical Engineering and Rail Transit, Changzhou University, Changzhou 213164, China*

Min Ji − *School of Mechanical Engineering and Rail Transit, Changzhou University, Changzhou 213164, China*

Feichi Zhang − *Institute for Technical Chemistry, Karlsruhe Institute of Technology (KIT), Karlsruhe 76128, Germany;* orcid.org/0000-0003-3260-5808

Jing Li − *School of Mechanical Engineering and Rail Transit, Changzhou University, Changzhou 213164, China*
Haijun Pan − *School of Mechanical Engineering and Rail Transit, Changzhou University, Changzhou 213164, China*
Yujie Zhao − *School of Mechanical Engineering and Rail Transit, Changzhou University, Changzhou 213164, China*
Zhen Zhang − *School of Mechanical Engineering and Rail Transit, Changzhou University, Changzhou 213164, China*

Notes

The authors declare no competing financial interest.

■ ACKNOWLEDGMENTS

The authors acknowledge the financial support from the National Natural Science Foundation of China (Project No. 51601021).

■ REFERENCES

(1) Vardhaman, B. S. A.; Amarnath, M.; Ramkumar, J. Experimental investigations to enhance the tribological behaviour of biodegradable oil by using manganese doped ZnO/FMWCNTs nanomaterials as lubricant additive. *Diamond Relat. Mater.* **2022**, *127*, No. 109155.
(2) Hou, L. Z.; Hou, M. F.; Yibibulla, T.; Mead, J. L.; Fatikow, S.; Wang, S. L.; Huang, H. Frictional shear stress of ZnO nanowires on natural and pyrolytic graphite substrates. *Friction* **2022**, *10*, 1237.
(3) Chai, Z. M.; Liu, Y. H.; Lu, X. C.; He, D. N. Influence of crystal structure on friction coefficient of ZnO films prepared by atomic layer deposition. *Sci. China Technol. Sci.* **2016**, *59* (3), 506−512.
(4) Sasaki, M.; Goto, M. Piezoelectric effect of crystal nanodomains on the friction force. *J. Vac. Sci. Technol. B* **2022**, *40*, No. 052803.
(5) Tan, D.; Xiang, Y.; Leng, Y. G.; Leng, Y. S. On the metal/ZnO contacts in a sliding-bending piezoelectric nanogenerator. *Nano Energy* **2018**, *50*, 291−297.
(6) Narasimulu, A. A.; Zhao, P. F.; Soin, N.; Prashanthi, K.; Ding, P.; Chen, J. K.; Dong, S. R.; Chen, L.; Zhou, E. P.; Montemagno, C. D.; Luo, J. Significant triboelectric enhancement using interfacial piezoelectric ZnO nanosheet layer. *Nano Energy* **2017**, *40*, 471−480.
(7) Zabinski, J. S.; Corneille, J.; Prasad, S. V.; McDevitt, N. T.; Bultman, J. B. Lubricious zinc oxide films: synthesis, characterization and tribological behaviour. *J. Mater. Sci.* **1997**, *32* (20), 5313−5319.
(8) Prasad, S. V.; McDevitt, N. T.; Zabinski, J. S. Tribology of tungsten disulfide-nanocrystalline zinc oxide adaptive lubricant films from ambient to 500 °C. *Wear* **2000**, *237* (2), 186−196.
(9) Prasad, S. V.; Zabinski, J. S. Tribological behavior of nanocrystalline zinc oxide films. *Wear* **1997**, *203*−*204*, 498−506.
(10) Nainaparampil, J. J.; Zabinski, J. S.; Prasad, S. V. Nanotribology of single crystal ZnO surfaces: Restructuring at high temperature annealing. *J. Vac. Sci. Technol. A* **1999**, *17* (4), 1787−1792.
(11) Goto, M.; Kasahara, A.; Tosa, M. Reduction in Frictional Force of ZnO Coatings in a Vacuum. *Jpn. J. Appl. Phys.* **2008**, *47* (12), 8914−8916.
(12) Goto, M.; Kasahara, A.; Konishi, Y.; Oishi, T.; Tosa, M.; Yoshihara, K. Frictional Property of Zinc Oxide Coating Films Observed by Lateral Force Microscopy. *Jpn. J. Appl. Phys.* **2003**, *42*, 4834−4836.
(13) Ren, K.; Liu, L.; Li, J.; Pan, H.; Wang, Z. Lubrication Behavior of n-hexadecane on ZnO Layer at the Nanoscale: A Molecular Dynamic Exploration. *Tribol. Lett.* **2022**, *70* (3), 90.
(14) Li, J.; Zhu, P.; Sheng, Y.-Y.; Liu, L.; Luo, Y. Atomistic simulations of the lubricative mechanism of a nano-alkane lubricating film between two layers of Cu−Zn alloy. *Chin. Phys. B* **2021**, *30* (8), No. 080205.
(15) Peng, J. F.; Yang, F. P.; Huang, K.; Dong, H.; Yan, S. A.; Zheng, X. J. Friction behavior of monolayer molybdenum diselenide nanosheet under normal electric field. *Phys. Lett. A* **2020**, *384* (7), No. 126166.
(16) Chen, X.; Huang, Y.; Zou, K.; Peng, Y. The controllable tuning of nanofriction on atomically thin hexagonal boron nitride with external electric field. *Appl. Surf. Sci.* **2022**, *581*, No. 152361.
(17) Gao, Y.; Xue, B.; Ma, L.; Luo, J. Effect of liquid crystal molecular orientation controlled by an electric field on friction. *Tribol. Int.* **2017**, *115*, 477−482.
(18) Senftle, T. P.; Hong, S.; Islam, M. M.; Kylasa, S. B.; Zheng, Y.; Shin, Y. K.; Junkermeier, C.; Engel-Herbert, R.; Janik, M. J.; Aktulga, H. M.; et al. The ReaxFF reactive force-field: development, applications and future directions. *npj Comput. Mater.* **2016**, *2* (1), 15011.
(19) Zhu, X.; Luo, Y.; Wang, X.; Jiang, Y.; Zhang, H.; Peng, Y.; Liu, Y. Probing Friction Properties of Hydrogen-Free DLC Films in a Nitrogen Environment Based on ReaxFF Molecular Dynamics. *Langmuir* **2022**, *38* (43), 13177−13186.
(20) Wang, Y.; Hayashi, K.; Ootani, Y.; Bai, S.; Shimazaki, T.; Higuchi, Y.; Ozawa, N.; Adachi, K.; De Barros Bouchet, M. I.; Martin, J. M.; Kubo, M. Role of OH Termination in Mitigating Friction of Diamond-like Carbon under High Load: A Joint Simulation and Experimental Study. *Langmuir* **2021**, *37* (20), 6292−6300.
(21) Yu, H.; Zheng, Z.; Chen, H.; Qiao, D.; Feng, D.; Gong, Z.; Dong, G. An investigation of tribochemical reaction kinetics from the perspective of tribo-oxidation. *Tribol. Int.* **2022**, *165*, 107289.
(22) Wang, P.; Duan, F. Tribochemistry of Graphene Oxide/Graphene Confined between Iron Oxide Substrates: Implications for Graphene-Based Lubricants. *ACS Appl. Nano Mater.* **2022**, *5* (9), 12817−12825.
(23) Thompson, A. P.; Aktulga, H. M.; Berger, R.; Bolintineanu, D. S.; Brown, W. M.; Crozier, P. S.; in 't Veld, P. J.; Kohlmeyer, A.; Moore, S. G.; Nguyen, T. D.; et al. LAMMPS - a flexible simulation tool for particle-based materials modeling at the atomic, meso, and continuum scales. *Comput. Phys. Commun.* **2022**, *271*, No. 108171.
(24) Martínez, L.; Andrade, R.; Birgin, E. G.; Martinez, J. M. PACKMOL: a package for building initial configurations for molecular dynamics simulations. *J. Comput. Chem.* **2009**, *30* (13), 2157−2164.
(25) Xu, J.; Nian, J.; Wang, P.; Guo, Z.; Liu, W. Elastic Lubricious Effect of Solidlike Boundary Films in Oil-Starvation Lubrication. *J. Phys. Chem. C* **2019**, *123* (3), 1677−1691.
(26) Wu, L.; Keer, L. M.; Lu, J.; Song, B.; Gu, L. Molecular dynamics simulations of the rheological properties of graphene-PAO nanofluids. *J. Mater. Sci.* **2018**, *53* (23), 15969−15976.
(27) Nosé, S. A molecular dynamics method for simulations in the canonical ensemble. *Mol. Phys.* **1984**, *52* (2), 255−268.
(28) Hoover, W. G. Canonical dynamics: Equilibrium phase-space distributions. *Phys. Rev. A* **1985**, *31* (3), 1695−1697.
(29) Stukowski, A. Visualization and analysis of atomistic simulation data with OVITO−the Open Visualization Tool. *Modell. Simul. Mater. Sci. Eng.* **2010**, *18* (1), No. 015012.
(30) Sengul, M. Y.; Randall, C. A.; van Duin, A. C. T. ReaxFF Molecular Dynamics Study on the Influence of Temperature on Adsorption, Desorption, and Decomposition at the Acetic Acid/Water/ZnO($10\bar{1}0$) Interface Enabling Cold Sintering. *ACS Appl. Mater. Interfaces* **2018**, *10* (43), 37717−37724.
(31) van Duin, A. C. T.; Dasgupta, S.; Lorant, F.; Goddard, W. A. ReaxFF: A Reactive Force Field for Hydrocarbons. *J. Phys. Chem. A* **2001**, *105* (41), 9396−9409.
(32) Rappe, A. K.; Goddard, W. A. Charge equilibration for molecular dynamics simulations. *J. Phys. Chem. A* **1991**, *95* (8), 3358−3363.
(33) van Gunsteren, W. F.; Berendsen, H. J. C. Algorithms for macromolecular dynamics and constraint dynamics. *Mol. Phys.* **1977**, *34* (5), 1311−1327.
(34) Wu, H.; Khan, A. M.; Johnson, B.; Sasikumar, K.; Chung, Y. W.; Wang, Q. J. Formation and Nature of Carbon-Containing Tribofilms. *ACS Appl. Mater. Interfaces* **2019**, *11* (17), 16139−16146.

(35) Liu, D. J.; Li, H. P.; Huo, L. X.; Wang, K.; Sun, K.; Wei, J. J.; Chen, F. Molecular dynamics simulation of the lubricant conformation changes and energy transfer of the confined thin lubricant film. *Chem. Eng. Sci.* **2023**, *270*, No. 118541.
(36) Ta, T. D.; Tieu, A. K.; Tran, B. H. Influences of iron and iron oxides on ultra-thin carbon-based tribofilm lubrication. *Tribol. Int.* **2022**, *173*, No. 107665.
(37) Ali, M. K. A.; Xianjun, H. Improving the heat transfer capability and thermal stability of vehicle engine oils using Al2O3/TiO2 nanomaterials. *Powder Technol.* **2020**, *363*, 48−58.
(38) Todd, B. D.; Daivis, P. J. *Nonequilibrium Molecular Dynamics: Theory, Algorithms and Applications*; Cambridge University Press, 2017.
(39) Jabbarzadeh, A.; Atkinson, J. D.; Tanner, R. I. Wall slip in the molecular dynamics simulation of thin films of hexadecane. *J. Chem. Phys.* **1999**, *110* (5), 2612−2620.
(40) Paniagua-Guerra, L. E.; Gonzalez-Valle, C. U.; Ramos-Alvarado, B. Effects of the Interfacial Modeling Approach on Equilibrium Calculations of Slip Length for Nanoconfined Water in Carbon Slits. *Langmuir* **2020**, *36* (48), 14772−14781.
(41) Auhl, R.; Everaers, R.; Grest, G. S.; Kremer, K.; Plimpton, S. J. Equilibration of long chain polymer melts in computer simulations. *J. Chem. Phys.* **2003**, *119* (24), 12718−12728.
(42) Tran, N. V.; Kiet Tieu, A.; Zhu, H.; Ta, H. T. T.; Sang, P. T.; Le, H. M.; Ta, T. D. Insights into the tribochemistry of sliding iron oxide surfaces lubricated by sodium silicate glasses: An ab initio molecular dynamics study. *Appl. Surf. Sci.* **2020**, *528*, No. 147008.
(43) Savio, D.; Fillot, N.; Vergne, P.; Zaccheddu, M. A Model for Wall Slip Prediction of Confined n-Alkanes: Effect of Wall-Fluid Interaction Versus Fluid Resistance. *Tribol. Lett.* **2012**, *46* (1), 11−22.
(44) Ta, D. T.; Tieu, A. K.; Zhu, H. T.; Kosasih, B. Thin film lubrication of hexadecane confined by iron and iron oxide surfaces: A crucial role of surface structure. *J. Chem. Phys.* **2015**, *143* (16), No. 164702.
(45) Ward, A.; Hilitski, F.; Schwenger, W.; Welch, D.; Lau, A. W.; Vitelli, V.; Mahadevan, L.; Dogic, Z. Solid friction between soft filaments. *Nat. Mater.* **2015**, *14* (6), 583−588.
(46) Mehrnia, S.; Pelz, P. F. Slip length of branched hydrocarbon oils confined between iron surfaces. *J. Mol. Liq.* **2021**, *336*, No. 116589.
(47) Cao, B.-Y.; Chen, M.; Guo, Z.-Y. Effect of surface roughness on gas flow in microchannels by molecular dynamics simulation. *Int. J. Eng. Sci.* **2006**, *44* (13−14), 927−937.
(48) Hilaire, L.; Siboulet, B.; Charton, S.; Dufreche, J. F. Liquid-Liquid Flow at Nanoscale: Slip and Hydrodynamic Boundary Conditions. *Langmuir* **2023**, *39* (6), 2260−2273.
(49) Kalin, M.; Polajnar, M. The Effect of Wetting and Surface Energy on the Friction and Slip in Oil-Lubricated Contacts. *Tribol. Lett.* **2013**, *52* (2), 185−194.
(50) Wang, Y. Z.; Yin, Z. Y.; Fan, D. K.; Bai, L. C. Friction behaviors of DLC films in an oxygen environment: An atomistic understanding from ReaxFF simulations. *Tribol. Int.* **2022**, *168*, 107448.
(51) Wang, Z. L.; Wang, A. C. On the origin of contact-electrification. *Mater. Today* **2019**, *30*, 34−51.
(52) Maritsa, L.; Martel, S.; Barros, R.; Bol, A.; Aparicio, S. Additivation of MoS2 nanosheets to synthetic poly-alpha-olefins base oils: A theoretical study of nanolubrication. *J. Mol. Liq.* **2021**, *332*, No. 115881.
(53) Ratoi, M.; Tanaka, H.; Mellor, B. G.; Sugimura, J. Hydrocarbon Lubricants Can Control Hydrogen Embrittlement. *Sci. Rep.* **2020**, *10* (1), No. 1361.
(54) Zhou, A.; Liu, X.-B.; Wang, Q.; Zhang, S.-Y.; Meng, Y.; Zhou, H.-B.; Zhang, S.-H. Investigation of nano-tribological behaviors and deformation mechanisms of Cu-Ni alloy by molecular dynamics simulation. *Tribol. Int.* **2023**, *180*, No. 108258.
(55) Seal, A.; Govind Rajan, A. Modulating Water Slip Using Atomic-Scale Defects: Friction on Realistic Hexagonal Boron Nitride Surfaces. *Nano Lett.* **2021**, *21* (19), 8008−8016.
(56) Restrepo, S. E.; van Eijk, M. C. P.; Ewen, J. P. Behaviour of n-alkanes confined between iron oxide surfaces at high pressure and shear rate: A nonequilibrium molecular dynamics study. *Tribol. Int.* **2019**, *137*, 420−432.